Hahn, Rodenacker, Auer:

Intensity Segmentation of the Human Brain with Tissue dependent Homogenization

Sonderforschungsbereich 386, Paper 296 (2002)

Online unter: http://epub.ub.uni-muenchen.de/

Intensity Segmentation of the Human Brain with Tissue dependent Homogenization ⋆

Klaus Hahn [a] Karsten Rodenacker [a] Dorothee P. Auer [b]

[a] *GSF-National Research Centre for Environment and Health, Institute of Biomathematics and Biometry, 85764 Neuherberg, Germany*

[b] *Max Planck Institute of Psychiatry, NMR study group, Munich, Germany*

Abstract

High-precision segmentation of the human cerebral cortex based on T1-weighted MRI is still a challenging task. When opting to use an intensity based approach, careful data processing is mandatory to overcome inaccuracies. They are caused by noise, partial volume effects and systematic signal intensity variations imposed by limited homogeneity of the acquisition hardware. We propose an intensity segmentation which is free from any shape prior. It uses for the first time alternatively grey (GM) or white matter (WM) based homogenization. This new tissue dependency was introduced as the analysis of 60 high resolution MRI datasets revealed appreciable differences in the axial bias field corrections, depending if they are based on GM or WM. Homogenization starts with axial bias correction, a spatially irregular distortion correction follows and finally a noise reduction is applied. The construction of the axial bias correction is based on partitions of a depth histogram. The irregular bias is modelled by Moody Darken radial basis functions. Noise is eliminated by nonlinear edge preserving and homogenizing filters. A critical point is the estimation of the training set for the irregular bias correction in the GM approach. Because of intensity edges between CSF (cerebro spinal fluid surrounding the brain and within the ventricles), GM and WM this estimate shows an acceptable stability. By this supervised approach a high flexibility and precision for the segmentation of normal and pathologic brains is gained. The precision of this approach is shown using the Montreal brain phantom. Real data applications exemplify the advantage of the GM based approach, compared to the usual WM homogenization, allowing improved cortex segmentation.

Key words: Segmentation, homogenization, nonlinear smoothing, radial basis function networks

⋆ This work was supported by DFG SFB 386.
Email address: Hahn@gsf.de (Klaus Hahn).

1 Introduction

At present two main streams of segmentation methods are apparent. On the one hand we find the data-based or bottom-up intensity segmentation, on the other hand the model-based or top-down approach, where often active contour models are fitted to some tissue boundaries (Szekeley and Gerig, 2000; MacDonald et al., 2000). The bottom-up methods use predominantly measured intensity information e.g. intensity values from T1-weighted MRI data which separate between brain tissue compartments and thus allow for a labelling of CSF, GM and WM voxels. However, because of tissue connections e.g. within the cortex foldings due to partial volume voxels or between different neuroanatomical structures this method alone is not sufficient for e.g. a cortex segmentation. In top-down approaches on the other hand lacking topological or geometrical information can be incorporated quite naturally. However, to fit an active contour model to the intensity edges between GM and WM or CSF, it is necessary to have a mainly correct labelling of these tissues. So, usually for a segmentation of neuroanatomical structures both approaches have to be combined (MacDonald et al., 2000; Dale et al., 1999), where essentially bottom-up preprocesses top-down.

This paper deals with a non parametric bottom-up method applying equally well to normal and pathologic brains as no implicit shape prior is involved. Though this approach is similar to others, see Dale et al. (1999) for a review, it introduces new insights and new methods which can improve bottom-up procedures. The approach proceeds in different steps to remove various artifacts produced by the scanning process. These steps are: correction of axial RF distortions, skull pealing (via, strictly spoken, a top-down tool), correction of spatially irregular distortions, edge preserving noise elimination and introduction of global thresholds to separate CSF, GM and WM voxels.

The analysis of 30 normal and 30 pathologic high resolution MRI datasets measured at 1.5 T showed that the usual assumption of tissue independency for distortion correcting bias fields (Wells et al., 1996; Sled et al., 1998) appears to be a very rough approximation. As will be demonstrated in detail, in the top and bottom regions of the brains the axial distortion correction functions differ by up to 20 %, depending if they are derived from WM or GM intensities. This indicates an appreciable tissue dependency in the bias fields. Such effects would surely increase with the field strength applied, e.g. in 3 T experiments, as in addition susceptibility distortions become more severe. This observation led us to introduce methods for distortion corrections which are tissue depended and can be based either on WM or on GM intensities. This concerns the axial correction, the irregular correction and the noise elimination. In addition, under the assumption of tissue independency, frequently WM is chosen to adapt a model for the bias fields (Dawant et al., 1993; Dale et al., 1999).

However, this leads to questionable extrapolations into GM regions. Therefore, as will be shown, a cortex segmentation can be essentially improved by the use of GM as training set for the bias fields. Having defined the methods, they are validated via the Montreal brain phantom (Mbp) (Cocosco et al., 1997; Kwan et al., 1996) and applications to realistic datasets are presented.

2 Materials and Methods

2.1 The Data

Establishing a method for improved segmentation of the cerebral cortex was felt necessary for an on-going study aiming to compare geometrical properties, namely the fractal dimension (V. Kiselev et al., Is the Brain Cortex a Fractal ?, submitted to NeuroImage) of the cerebral cortex in healthy and schizophrenic brains. There were 60 MRI datasets available from 30 normal and 30 schizophrenic brains which had been acquired at 1.5 T (Signal Echospeed, GE Medical Systems) using a standard head coil and an inversion recovery prepared T1 weighted spoiled gradient echo recalled sequence (SPGR) with the following parameters: repetition time (TR) = 10.3 ms, echo time (TE) = 3.4 ms, field of view (FOV) = 23 x 23 cm^2, matrix size = 256 x 256, flip angle = 20^0. The three-dimensional data set consists of 128 contiguous sagittal slices with varying slice thickness (1.2 - 1.4 mm) according to head size. In addition, to exemplify the flexibility and robustnessof the segmentation approach, an identically acquired dataset from a grossly malformed brain with moderate motion artifacts was included. All datasets were anonymized prior to transfer and further analysis and all subjects undergoing non clinical examinations had given written informed consent prior to study participation.

2.2 Skull Pealing

First the skull and non brain tissue must be removed from the raw data sets. To achieve this a three dimensional active contour procedure is applied: After a start ellipsoid is placed inside the WM, an implicit surface polygonizer (Bloomenthal, 1994) calculates a polygonal approximation to the ellipsoidal surface and determines the vertices, $\vec{X}_k$, and outward normal vectors, $\vec{N}_k$. The vertices are shifted outside in n iterations in direction of the normal vectors according to the active contour equation Eq. 1, adapting the ellipsoid to the surface of the brain:

$$\overrightarrow{X}(n+1) = \overrightarrow{X}(n) + \overrightarrow{Force}_{Regularization}(n) + \overrightarrow{Force}_{\vec{N}_k}(n) \quad (1)$$

The forces defined in Dale et al. (1999) are used. The parameters were adapted to the processed datasets. The procedure is stopped, when the contour reaches the low CSF intensity valleys near the skull. As the contour is in general a non convex surface, a ray crossing algorithm (Rourke, 1998) is applied to find the points inside. This method counts for a random ray the number of contour crossers, which is odd for insiders and even else. Frequently, for a proper regularization strength in Eq. 1 the cerebellum is not completely inside the contour as it demands high curvature. This can be improved by the use of a second start ellipsoid spanning the back side of the brain volume. However, as the cerebellar surface foliae are less well resolved at 1.5 T measurements and are not in the focus of our application problem, the cerebellum is not included into our analysis. Together with some remaining skin artifacts, it is removed interactively by restricted orthogonal slicing.

2.3 Tissue dependent corrections of axial distortions

As second step the intensity distortions due to susceptibility effects or RF field inhomogeneities are corrected. The axial component is treated separately by a new routine for estimation of the axial intensity correction function. The routine can be applied for estimation of GM as well as WM related correction functions. This correction function $c(z)$ defines for each axial depth z a characteristic intensity value of a common tissue component, e.g. WM. Correction is performed for all points of an axial slice with coordinate z by

$$\text{Intensity}_{\text{corr}}(z) = \text{Intensity}(z)\frac{\max_z\{c(z)\}}{c(z)} \tag{2}$$

Given the axial intensity histograms $f(z,i)$ with $z \in Z$, the axial coordinate range and $i \in I$, the intensity range (see Fig. 1 A), we call f the depth histogram. This depth histogram is smoothed by a moving average of window size 1 x 5 [a.u.] (pure intensity smoothing, maximum intensity $\approx$ 150 [a.u.]). On the basis of all local maxima and minima of $f(z,i)$ each histogram is divided into subintervals containing the respective local maximum and limited by the neighboring minima (see Fig. 1 B). This results in a partition $\mathcal{P}(z)$ of the intensity interval I per axial coordinate z. We use for fully automatic calculation a 1-dimensional watershed algorithm (Serra, 1982; Vincent and Soille, 1991). To obtain a WM or GM related correction function, the starting point (subinterval) $P(z_0,i_0)$ is interactively selected in the displayed depth histogram (see Fig. 1 A). From this subinterval $P(z_0,i_0) \in \mathcal{P}(z_0)$ an iteration is started in upper and lower axial direction (left and right in Fig. 1 A) where the neighboring subinterval $P(z,i)$ is selected with maximum intersection $(P(z_0,i_0) \cap P(z,i))\ \forall i; P(z,i) \in \mathcal{P}(z)$. The intensity of this (unique) local maximum in the selected subinterval is the value of the correction func-

tion $c(z)$. Choosing the local maximum minimizes the influence of falsifying partial volume voxels. Resulting correction functions calculated from WM or GM starting points after skull pealing are plotted into the displayed depth histograms in yellow (WM) and blue (GM) (Fig. 2).

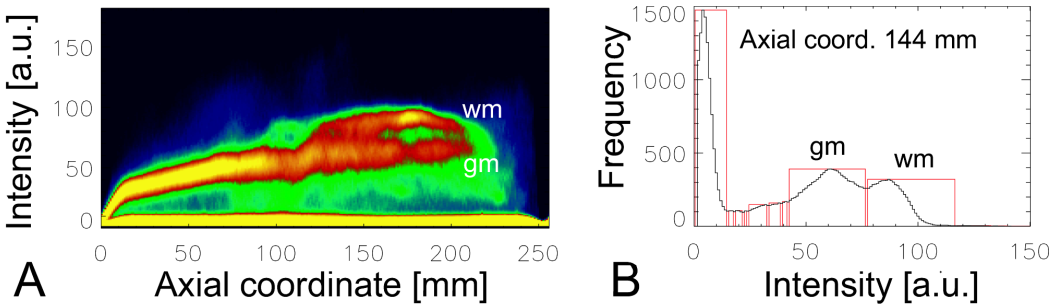

Fig. 1. Depth histogram with red-yellow indicating high and blue-green indicating low frequencies (A). Histogram and partition with local maxima outlined in red(B). Skull pealing not yet performed. The axial coordinate range 130-210 corresponds to the anatomic range "cerebellum" - "top of the head".

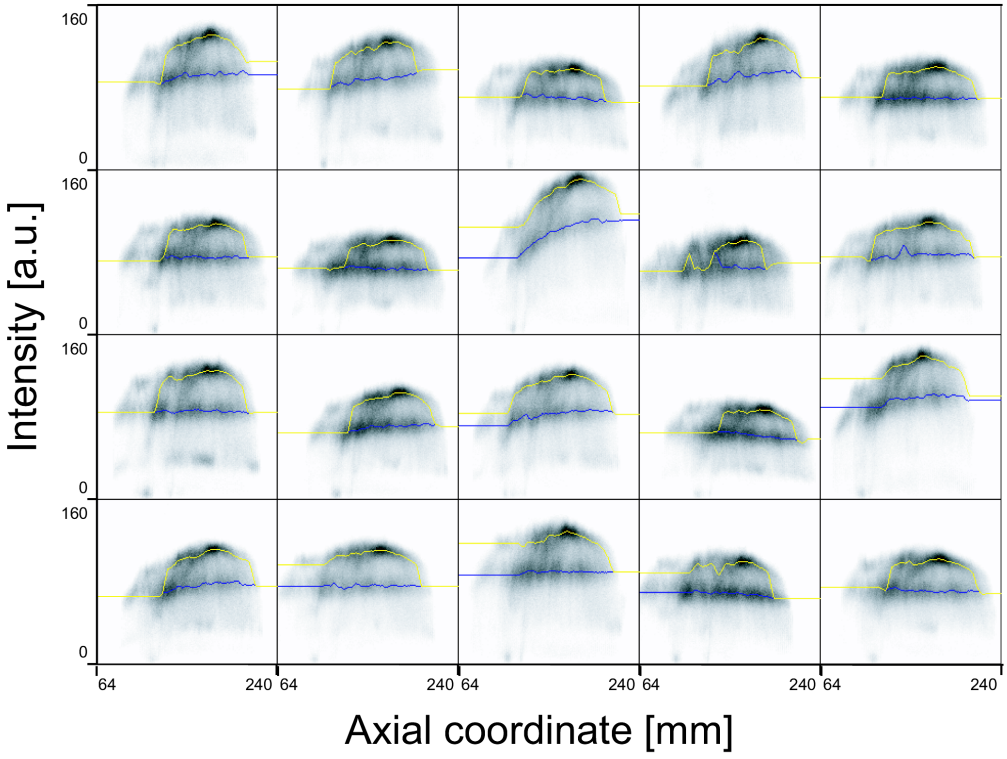

Fig. 2. Depth histograms for 20 brains after skull pealing. Correction functions for GM (blue) and WM (yellow) are indicated. Grey scale represents the frequency.

From the analysis of the WM and GM based correction functions we find a different behavior in axial direction. This can be observed in Fig. 2 and is

quantified in the plot of the normalized ratios of the two corresponding correction functions (Fig. 3). The ratios indicate an appreciably smaller relative distortion of GM intensities than that of WM in the top and bottom regions of the brain.

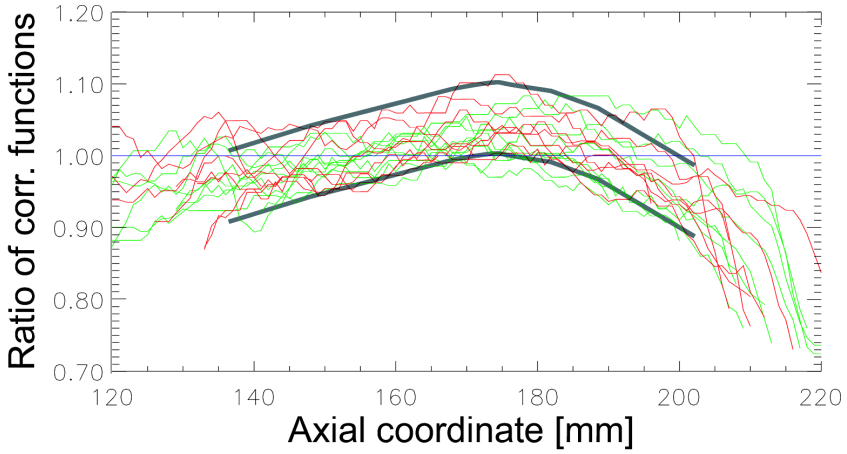

Fig. 3. Normalized ratios of correction functions $\frac{c_{WM}(z)}{c_{GM}(z)} \frac{max_z(c_{GM}(z))}{max_z(c_{WM}(z))}$ for the brains of Fig. 2. Similar behavior in normal (green) and schizophrenic (red) brains is apparent. To guide the eye qualitative trends are indicated by thick lines.

This tissue dependency may be partly due to variations of the horizontal components in the bias field causing different axial dependency for inner (WM) or outer (GM) regions. Another reason may be found in susceptibility effects which are more effective at the frontal region of the head than in WM. For strongly distorted data it is sometimes more convenient to apply the axial bias correction before skull pealing to homogenize the intensity levels. The corresponding normalized ratios for 60 brains are presented in Fig. 4 with no apparent difference compared to Fig. 3. For both cases we find a maximum 10 - 20 % deviation in the ratios of correction functions. Compared to a tissue independent approach like in Dale et al. (1999) the application of specific correction functions improves the homogenization of the corresponding tissue compartment, preparing an improved segmentation via thresholding.

2.4 Tissue dependent corrections of irregular distortions

In a third step the residual spatially irregular bias is removed. Again tissue dependent methods are introduced. In good approximation we can now assume that CSF, GM and WM are separated by intensity steps. Accordingly not only WM but also GM offers a natural training set for a neuronal network estimating the bias field. To achieve this, the brain volume enlarged by a convenient boundary layer is covered by a Moody-Darken expansion of three

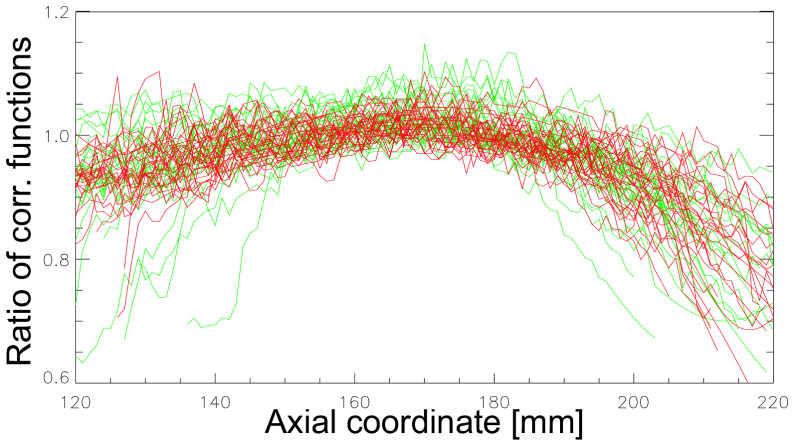

Fig. 4. Normalized ratios of correction functions for 60 brains without skull pealing. Normal (green) and schizophrenic (red) brains are presented.

dimensional radial basis functions (Moody and Darken, 1989; Bishop, 2000) modeling a smooth distortion trend $T(\vec{x})$ in the brain volume:

$$T(\vec{x}) = \sum_{i=1}^{N} w_i \, e^{-\frac{(\vec{x}-\vec{m}_i)^2}{2\sigma^2}} \Big/ \sum_{i=1}^{N} e^{-\frac{(\vec{x}-\vec{m}_i)^2}{2\sigma^2}} + w_0 \tag{3}$$

For our data set the centers $\vec{m}_i = (m_i^1, m_i^2, m_i^3)$ are regularly spaced at a distance $|m_i^j - m_{i+1}^j| \approx 20 - 30$ mm and for the basis functions a width $\sigma \approx 20 - 25$ mm is used, depending on the size (age) of the brain. Applying a GM or WM based correction, the bias w_0 is identified with the corresponding tissue peak of the global intensity histogram. The linear weights w_i are adapted by minimization of an error function which is defined on the tissue dependent training set of intensity values $data(\vec{y})$:

$$\min_{\{w\}} \left[\sum_{\vec{y} \in \text{GM or WM}} (T(\vec{y}) - \text{data}(\vec{y}))^2 + \alpha \sum_{i=1}^{N} w_i^2 \right] \tag{4}$$

In the penalty regularization term a constant $\alpha = 10$ was used. Compared to the standard RBF model without normalization the Moody and Darken (1989) variant produces better extrapolation properties. To perform the high dimensional minimization numerically, a stable conjugate gradient algorithm, avoiding the use of second derivatives, is applied (Press et al., 1992).

The trend model Eq. 3 can be considered as a generalization of a linear Gaussian filter for the brain volume averaging on a large scale only GM or WM distortions, details of this earlier used method can be found in Hahn et al. (2000). In comparison to the linear filter the network has several advantages: The stiffness of the trend can be controlled by α, the smoothness by N and σ; once adapted weights can be used as starting values for another brain with

similar size which was scanned under similar circumstances. In contrast to e.g. a cortex homogenization based on WM data, the GM based procedure does not extrapolate specific distortions to GM, but uses essentially an approximation within the GM region.

In both approaches reliable estimates of the corresponding training set, being subsets of GM or WM must be found. This is more delicate for GM training, as two separations are necessary. To find reasonable global separating thresholds, the probability density d of the global image intensities is used. First, the GM or WM peaks P_g or P_w are located automatically by a maximization within given limits. For GM as training set, the lower and upper global thresholds g_i, $i = \{low, high\}$, are given then by the intensities closest to P_g with $d(g_i) = c_i d(P_g)$. The weights $c_i < 1$ are mainly dependent on the scanner modalities and quite stable. Most of the brains which are analyzed so far could be segmented with $c_{low} \approx .7$ and $c_{high} \approx .8$. To reduce classification errors a high c value is convenient, to achieve a representative training set low values shall be used, c should approximately optimize this trade off. For white matter training $c_{low} \approx .7$ with respect to P_w was convenient. These c values must be found interactively on the basis of test slices, see Fig. 11 for examples.

The total bias correction is performed iteratively. After calculation of the trend $T(\vec{x})$ via Eq. 4 the intensity in the whole brain is corrected similar to the axial case (Eq. 2) by

$$\mathrm{data}_{\mathrm{corrected}}(\vec{\mathrm{x}}) = \mathrm{const}\ \frac{\mathrm{data}(\vec{\mathrm{x}})}{\mathrm{T}(\vec{\mathrm{x}})} \tag{5}$$

The parameter `const` can be used to adjust the global intensity distribution. Iterating this procedure enlarges the thresholded volume of GM or WM and homogenizes the intensity in the brain. In the set of brains which were segmented, after 4 iterations a reasonable convergence was reached.

To illustrate the quality of the bias correction, results which were calculated with the Mbp (Cocosco et al., 1997; Kwan et al., 1996) are presented. From these simulated MRI volumes, sets of T1-weighted images were used with the following data characteristics: 181x271x181 voxels of 1x1x1 mm^3, field strength 1.5 T, spoiled Flash sequence, with a 30^o flip angle, 18 ms repeat time, 10 ms echo time. The noise level applied was 3 % of the intensity maximum, the distortion was 40 % RF nonuniformity, which roughly approximates the conditions in our real data sets. Anatomically the brain is modelled by CSF, WM and GM including glial tissue. As compared to WM training GM training based correction is more critical, therefore this case will be presented in detail. In Fig. 5 global intensity histograms for the distorted brain phantom Ph-3-40, for it's axial correction and for four bias corrections are shown. These procedures increase the homogenization, separating the CSF, GM and WM

peaks, (from left to right), more and more. Also the convergence of the iterated bias correction can be seen.

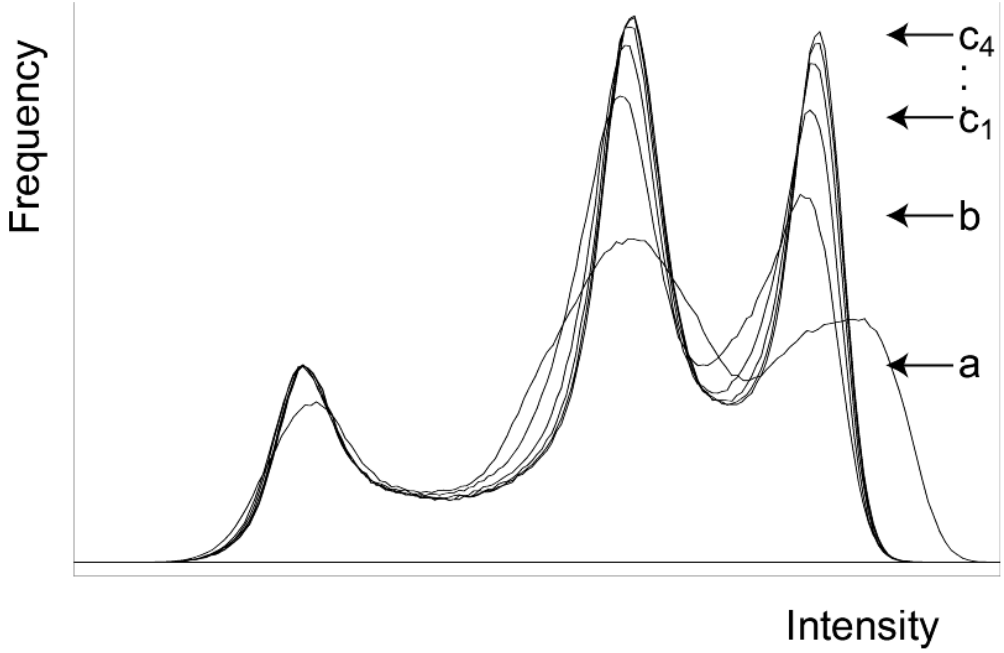

Fig. 5. Global intensity histograms based on GM corrections of Ph-3-40; a: Ph-3-40 for anatomy given in text, b: axially corrected, c_i : iteratively bias corrected.

In Fig. 6, for an axial slice, the true bias correction field calculated by the ratio Ph-0-0/Ph-0-40 and its estimate based on Ph-3-40 can be compared. In this notation Ph-0-0 stands for the phantom with no noise or distortion and Ph-0-40 for the phantom with 40 % distortion only. For the whole brain in Fig. 7 a scatterplot of the true bias field versus its estimate is shown. In addition, on the coordinate axes the frequency histograms of the individual bias correction fields are plotted. The distributions and the two dimensional scatter frequencies demonstrate a good agreement between phantom bias and estimate. The scatter frequency is linearly well aligned to the diagonal, few highly biased voxels, for a bias greater then 1.3, are slightly overestimated.

2.5 Tissue dependent denoising

In a fourth step, a last homogenization of the intensities is performed. It is coupled to the elimination of noise. To avoid blurring in the tissue transitions, a nonlinear edge preserving filter is used. The applied construction uses a chain of sigma filters, with well defined parameter modifications (Aurich and Weule, 1995; Winkler et al., 1999). Only two parameters must be specified by the user: first, the variance of the noisy data set, second the number of iterations, which controls the trade off between resolution and contrast enhancement.

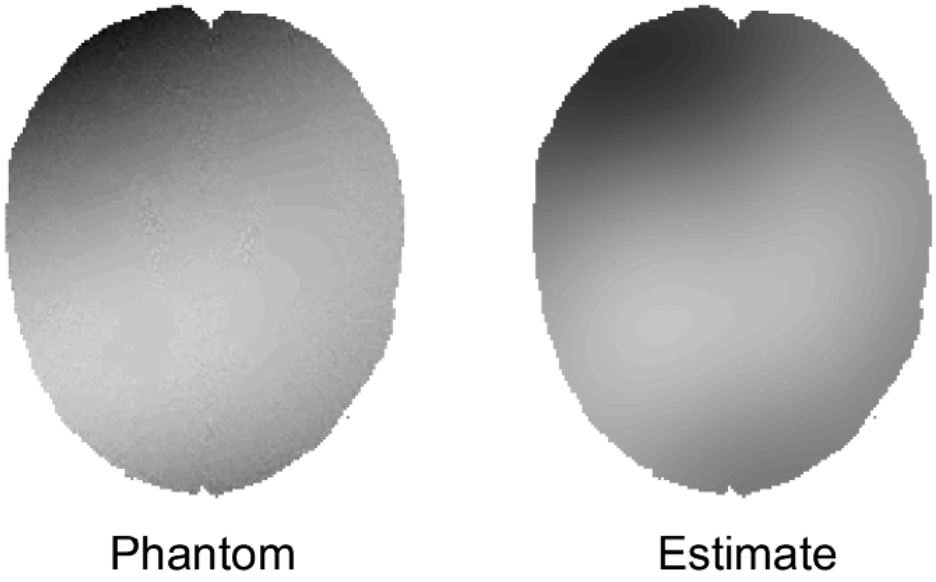

Fig. 6. Bias correction fields for an axial slice. Grey values indicate different heights (a.u.).

The numerical procedure consists essentially of a three dimensional averaging in space, limited by the nonlinear intensity window which enforces a tissue dependent smoothing. The chain is numerically stable, fast and statistically robust with respect to deviations from Gaussian noise. For three iterations the procedure can be formulated like follows:

$$
\begin{aligned}
F_\sigma^\tau(\text{intensity})(\vec{x}) &= \frac{1}{\text{norm}} \sum_{\vec{y} \in \substack{\text{neighbour} \\ \text{hood}(\vec{x})}} e^{-\frac{(\vec{x}-\vec{y})^2}{2\sigma^2}} e^{-\frac{(\text{intensity}(\vec{x})-\text{intensity}(\vec{y}))^2}{2\tau^2}} \text{intensity}(\vec{y}) \\
\text{intensity}^{\text{smooth}}(\vec{x}) &= F_{1.59^2\sigma}^{(\tau/3)/2} \circ F_{1.59\sigma}^{\tau/3} \circ F_\sigma^\tau(\text{intensity})(\vec{x})
\end{aligned}
\tag{6}
$$

σ is 70 % of the voxel width and $\tau/3$ the standard deviation of the noise in the image intensity. This parameterization produced in all cases a smoothing quality like that exemplified in the sagittal profile of Fig. 8. The increased homogenization of the CSF, GM and WM intensity levels by application of the chain is demonstrated in the global histograms of Fig. 9. In a final step the cortex is segmented by two global thresholds (see Fig. 9), which were adjusted by visual inspection of some brain slices. The method described in Sec. 2.3-2.5 applies equally well to WM based training data. As the Mbp contains per construction only tissue independent RF inhomogeneities, the then derived global histograms are very similar to those based on the GM training, see Hahn et al. (2001b,a) for corresponding Figures.

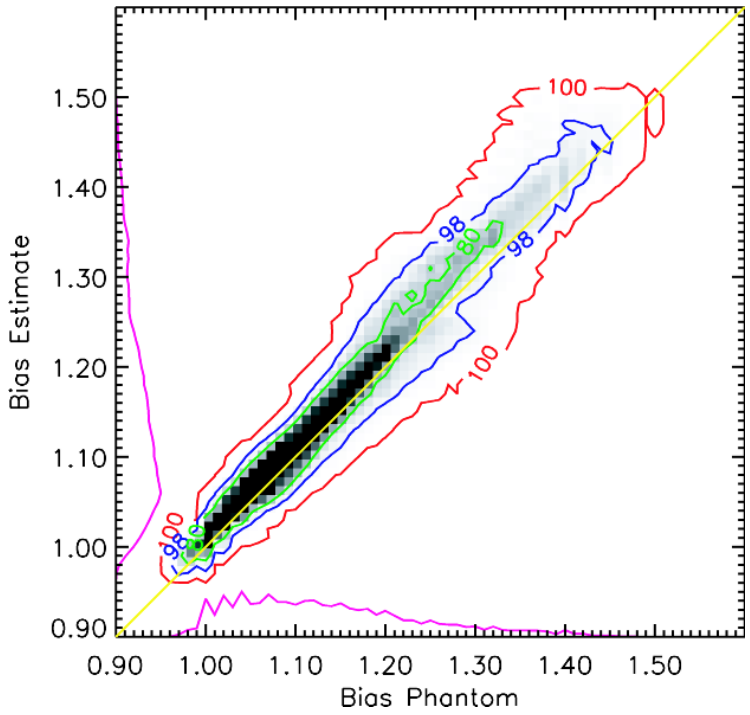

Fig. 7. Scatterplot of bias correction for the phantom and its estimate. Contours for 100, 98 and 80 % of the voxels are given in red, blue and green. Increasing grey level in the two dimensional distribution corresponds to an increase in the number of voxels. The corresponding one dimensional bias distributions are shown in violet above the axes. The diagonal (yellow) indicates the line of perfect agreement

Before thresholding, real data with a coarse grid resolution which are segmented for the purpose of a fractal dimensional analysis are regridded from width d to $d/2$ and smoothed by a Gaussian filter with standard deviation $\sigma = d/2$. This reduces minor irregular blocking effects at the boundaries caused by partial volume voxels and smoothes the surfaces between GM, WM and CSF.

3 Results

The presented algorithms were developed and iteratively improved within a period of about two years, some preliminary results are published in proceeding articles and abstracts (Hahn et al., 2000, 2001b,a). For test purposes more than 50 complete segmentations, partially for identical brains, were performed. Detailed analysis of the segmentation result using GM derived bias fields compared with the anatomical knowledge applied to the raw data was performed in 10 cases. In all subjects, segmentation was judged to very satisfactory label cortical structures with few misclassifications of single pixels corresponding to very thin WM or CSF spaces intermingled in cortical structures as GM. Also

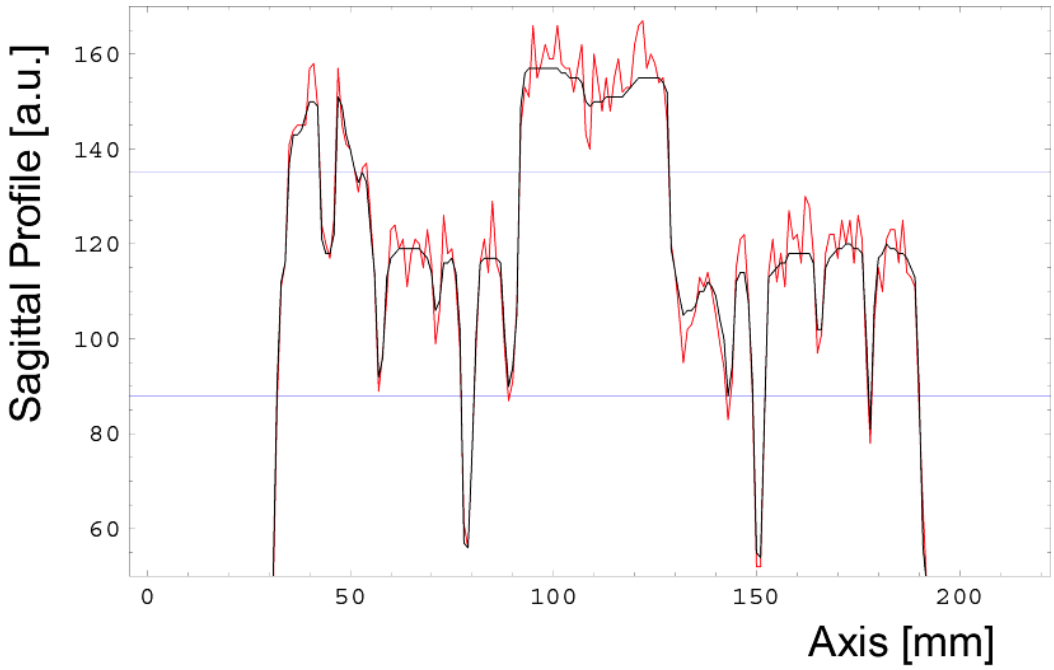

Fig. 8. Sagittal profile before smoothing (red, see Fig. 5: c_4) and after application of the filter chain (black, see Fig. 9: d_3). Thresholds enclosing GM are indicated by horizontal lines

the amygdala/hippocampal region was always well delineated by the segmentation algorithm even in two cases where the raw images showed superimposed image artifacts, namely curvilinear, sharp signal intensity variations probably due to ocular motion. Segmentation of the subcortical GM was however less efficient as could be expected for a pure bottom-up approach based on one contrast modality only. Whereas the caudate nucleus, anterior putamen and medial thalami were generally well segmented, correct classification of the tail of the putamen, globus pallidus and lateral parts of the thalami could not be sufficiently segmented.

The Mbp, Ph-3-40, was used for further quantitative validation. Like in Ashburner and Friston (2000) a κ statistics, measuring the segmentation quality for the whole brain, was calculated. The limiting values of κ indicate for $\kappa = 0$ statistical independency between segmentation result and phantom and for $\kappa = 1$ perfect dependency or agreement. We found for the control case of the phantom with no noise and distortions, Ph-0-0, the value $\kappa = 0.985$, reflecting the limit of an application of global thresholding to the Mbp. For the distorted phantom, Ph-3-40, we found an improvement from $\kappa = 0.913$ after thresholding to $\kappa = 0.962$ after application of the described GM homogenization and then thresholding. The same κ value was achieved for WM homogenization as the Mbp contains only tissue independent distortions. This κ value indicates a high segmentation quality, in a similar application by the SPM method (Ashburner and Friston, 2000) a value of $\kappa = 0.95$ is reported. A comparison for

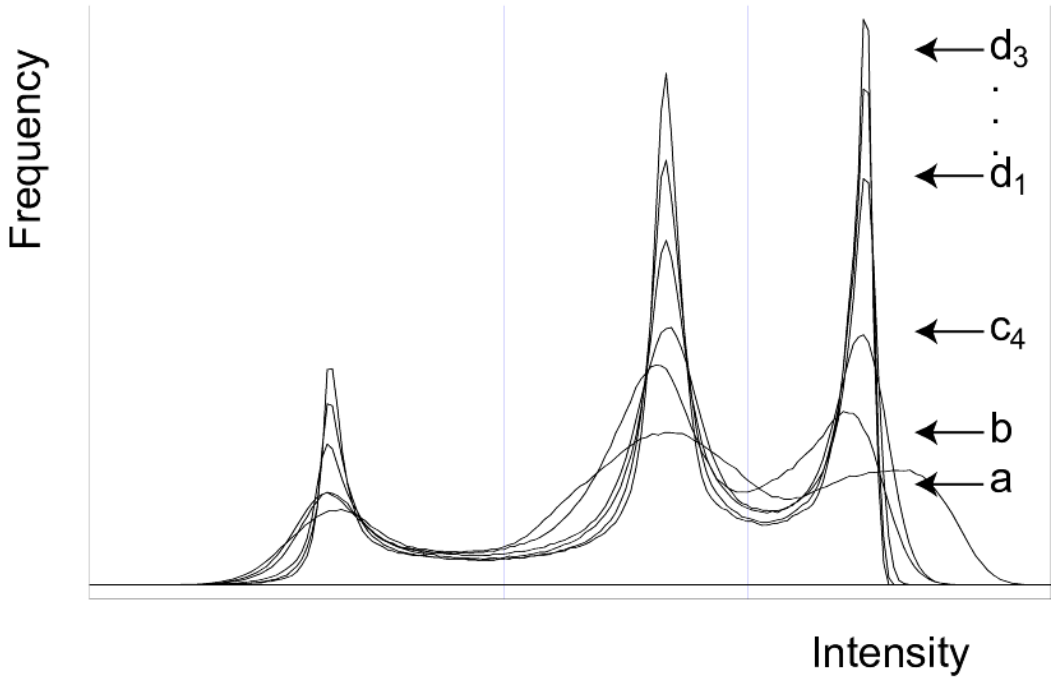

Fig. 9. Global intensity histograms based on Ph-3-40. For a - c see Fig. 5, d_i : iteratively smoothed data starting from level c_4 by the filters of Eq. 6. The vertical bars indicate global thresholds, separating (from left to right) CSF, GM and WM.

a representative axial and sagittal slice of the phantom and the GM segmentation result is shown in Fig. 10, illustrating the high quality of the method. Similar quality is achieved for the WM approach.

Results for GM and WM homogenization of a representative realistic brain illustrate the differences for both approaches, see Fig. 11, panel A, for global intensity histograms. The frequency distributions for three successive processing steps: axial correction, irregular bias correction and denoising are shown. Depending on the initial tissue chosen, the homogenization is increased mainly for GM or WM, leading to an accentuation of the corresponding intensity maximum. In Fig. 11, panel B and C, GM and WM training sets are shown for a coronal slice of this brain. In both cases the left panels show the training sets for the first irregular bias correction, the right panels the four times corrected sets achieved with the same thresholds. The volumes of the data sets grow and improve the presentation of the corresponding tissue due to increased homogenization, noise is not yet eliminated.

In Fig. 12 segmentation results for the same coronal slice are presented. Panel A shows the raw data intensities, panel B the GM based segmentation for the thresholds indicated in Fig. 11, panel A. Lower panels give results achieved with WM based segmentation. In panel C the grey-white threshold is chosen in such a way (high threshold in Fig. 11, panel A), that the grey-white interdigitation in the lower part of the brain is of the same quality like in the GM

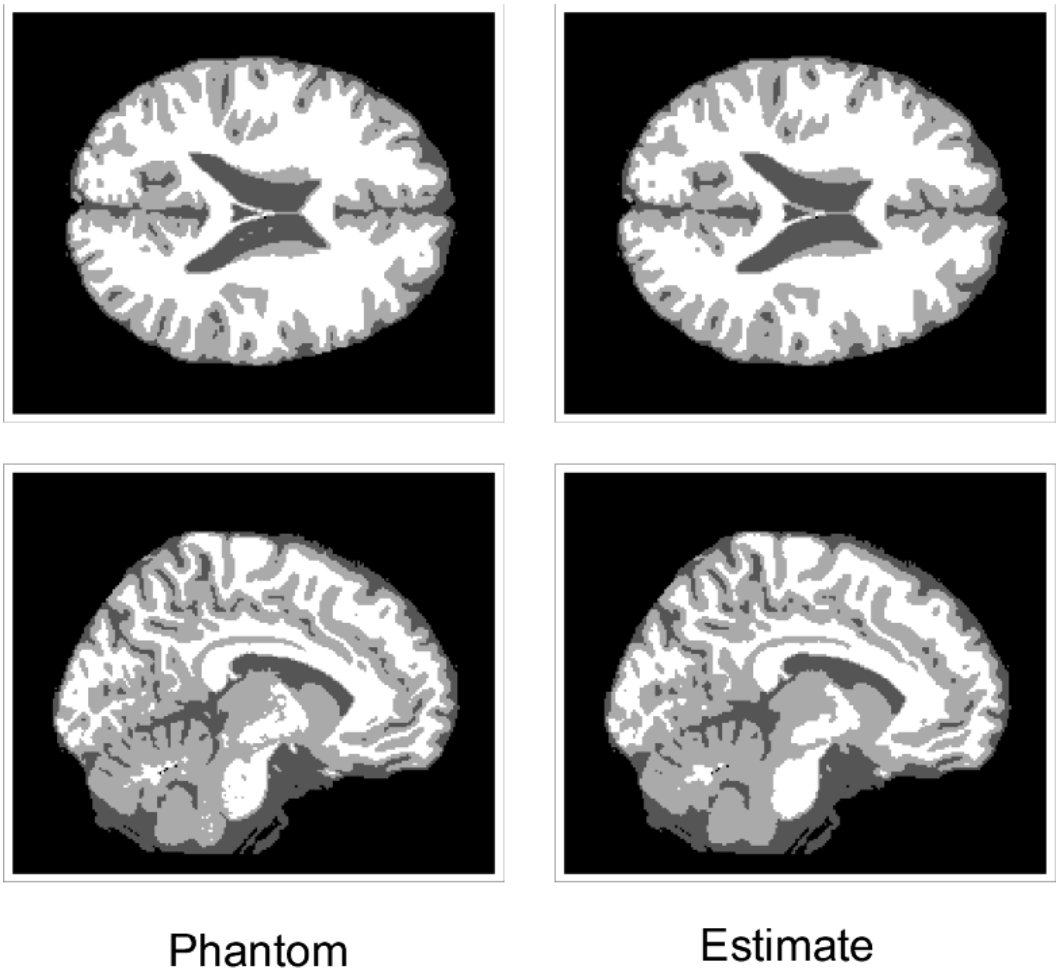

Fig. 10. CSF, grey and white matter of an axial and a sagittal slice in obvious coloring. Left panels show the labelling of the Montreal brain phantom, right panels the thresholded result of the segmentation method applied to Ph-3-40

based segmentation. Note the unrealistic zero cortex thickness in the apical region. In panel D the situation was reversed (middle threshold in Fig. 11, panel A), leading to an unrealistic increase of GM in the right lower part of the slice. Concluding, GM based segmentation is not only technically possible but indeed shows advantages, compared to the traditional WM based method, see Hahn et al. (2001b,a) for similar earlier derived results.

4 Discussion

A bottom-up segmentation without any shape prior is presented, based either on WM or GM homogenization. Advantages of the GM approach for cortex segmentation are found in 1.5 T data sets because of tissue dependent bias field inhomogeneities. The main intention for this approach is to increase flexibility

and precision of intensity segmentation, the price to pay is a lack of full automaticity. After application of the complete method to normal and pathologic brains the necessary supervision can be characterized as follows: Except for the parameters of the bias field estimation, the residual user interactions for a) skull pealing (positioning of the start ellipsoid, parameterization of Eq. 1 and application of the orthogonal slicing procedure), b) axial distortion correction (one-click GM or WM selection), c) smoothing (determination of the noise level) and d) determination of the global thresholds are quite trivial interactions which can usually be performed per brain within 15-30 minutes, when a convenient visualization software like IDL [1] or Mathematica [2] is used.

The bias field parameters Δm, σ and c_i are somewhat more delicate. The parameters Δm and σ are still relatively stable and vary in the range between 20-30 respectively 20-25 mm depending on the different brains considered. An adequate estimation of the training sets via c_i is a critical step as these sets should be both representative and mainly free from misclassified voxels. To achieve an optimal segmentation, this parameterization should be accompanied by visual checks of selected slices like those shown in Fig. 11. To give an example for the stability of c_i, the brain used for Fig. 11, 12 was segmented twice for $c_{low} = .6$ and .7 and $c_{high} = .75$ and .85 in the first iteration which is most critical. Though the separating thresholds of the training sets differ by about 5 % in the two runs, the segmented tissue labelling was nearly equivalent. This stability is preserved as long as the thresholds are essentially within the intensity steps separating CSF, GM and WM.

In standard cases bottom-up preprocesses top-down (see Sec. 1). Top-down approaches, however, are only applicable if a priori assumptions based on anatomical knowledge, like expected cortex thickness or moderate cortex curvature (MacDonald et al., 2000), are valid. In pathological cases such assumptions can be violated, namely by gross deviation from normal gyral and sulcal pattern including severalfold increase of cortical thickness, as shown in Fig. 13. The depicted case combines schizencephaly and pachygyria. In such cases only bottom-up methods can be applied. Though the dataset was additionally corrupted by structured noise caused by moderate head movement, the presented segmentation result based on GM homogenization is of good quality demonstrating the flexibility of the method. Concerning robustness, we found that only the parameters c_i had to be adjusted, the other parameter settings agree with that for the brain shown in Fig. 11, 12.

Though the present method produces satisfying results, it may be improved in several respects. Partial volume effects are not treated properly up to now, an example of a recent approach to this problem within the frame of intensity

[1] Interactive Data Language, Research Systems Inc., Boulder, Colorado, USA
[2] Wolfram Research Inc., Champaign, IL 61820-7237, USA

segmentation is given in Leemput et al. (2001). Further, the tissue separation by global thresholds may appear quite primitive. However, trials with a more advanced semiautomatic "adaptive region growing segmentation" (Pohle and Tönnies, 2001), where the necessary homogenization conditions for the tissue separation is learned in a first run before segmentation, did not bring any improvement. A recent approach by Grabowski et al. (2000), where a local segmentation by a mixture model, including partial volume effects, is applied, may be more convenient.

Finally, the method seems to be appropriate for data measured with higher field strength, e.g. with 3 T (see Sec. 1). In this case, essentially the susceptibility effects should increase. RF field inhomogeneities are then probably superimposed by strong susceptibility effects on possibly different spatial scales. To cope with this situation the full parameterization power of the radial basis function approach, which allows the use of space dependent Δm and σ, should be convenient. Applications to such data sets would be interesting studies for the future.

The involved numerical algorithms are programmed in C, Fortran90 and IDL and can be delivered on request.

Acknowledgement: We thank Prof. Dr. V. Aurich for his kind interest and especially for stimulating ideas concerning denoising methods.

References

Ashburner, J., Friston, K. J., 2000. Voxel-based morphometry - The methods. NeuroImage 11, 805–821.

Aurich, V., Weule, J., 1995. Non-linear gaussian filters performing edge preserving diffusion. In: Proc. 17. DAGM-Symposium. Springer, Bielefeld, pp. 538–545.

Bishop, C. M., 2000. Neural Networks for Pattern Recognition. University Press, Oxford.

Bloomenthal, J., 1994. An implicit surface polygonizer. In: Heckbert, P. S. (Ed.), GraphicsGems IV. AP Professional-Academic Press, Massachusetts, pp. 324–349.

Cocosco, C. A., Kollokian, V., K.S., K. S. K., et. al., 1997. Brainweb: Online interface to a 3D MRI simulated brain database. NeuroImage 5, 425.

Dale, A. M., Fischl, B., Sereno, M. I., 1999. Cortical surface-based analysis: 1. segmentation and surface reconstruction. NeuroImage 9, 179–194.

Dawant, B. M., Zijdenbos, A. P., Margolin, R. A., 1993. Correction of intensity variations in MR images for computer aided tissue classification. IEEE Trans. Med. Im. 12 (4), 770–781.

Grabowski, T. J., Frank, R. J., Szumski, N. R., 2000. Validation of partial tis-

sue segmentation of single-channel magnetic resonance images of the brain. NeuroImage 12, 640–656.

Hahn, K., Rodenacker, K., Auer, D. P., 2001a. Cortex homogenization for intensity segmentation - an alternative. NeuroImage 13 (6), 141.

Hahn, K., Rodenacker, K., Aurich, V., Auer, D. P., 2000. Segmentierung des Gehirns auf der Basis von MR-Daten. In: Horsch, A., Lehmann, T. (Eds.), Proc. Bildverarbeitung in der Medizin 2000. Springer, Berlin, pp. 86–90.

Hahn, K., Rodenacker, K., Kempe, A., Auer, D. P., 2001b. Intensitätssegmentierung von T1-Gewichteten MR Gehirndaten über die Homogenisierung der grauen oder weissen Materie - eine vergleichende Studie. In: Handels, H., Horsch, A., Lehmann, T., Meinzer, H.-P. (Eds.), Proc. Bildverarbeitung in der Medizin 2001. Springer, Berlin, pp. 207–211.

Kwan, K. S., Evans, A. C., Pike, G. B., 1996. An extensible MRI simulator for postprocessing evaluation. In: Proc. Conference on Visualistion in Biomedical Computing. pp. 135–140.

Leemput, K. V., Maes, F., Vandermeulen, D., et al., 2001. A statistical framework for partial volume segmentation. In: Proc. Medical Image Computing and Computer-Assisted Intervention-MICCAI. Springer, pp. 204–212.

MacDonald, D., Kabani, N., Avis, D., Evans, C., 2000. Automated 3-D extraction of inner and outer surfaces of cerebral cortex from MRI. NeuroImage 12, 340–356.

Moody, J., Darken, C. J., 1989. Fast learning in networks of locally-tuned processing units. Neuronal Comp 1 (2), 281–294.

Pohle, R., Tönnies, K. D., 2001. Segmentation of medical images using adaptive region growing. In: Proc. of SPIE (Medical Imaging 2001). SPIE, San Diego, pp. 1337–1346.

Press, W. H., Teukolsky, S. A., Flannery, B. P., et. al, 1992. Numerical Recipes. University Press, Cambridge.

Rourke, J. O., 1998. Computational Geometry in C, 2nd Edition. University Press, Cambridge.

Serra, J., 1982. Image analysis and mathematical morphology. Academic Press Inc., London u.a.

Sled, J. G., Zijdenbos, A. P., Evans, C., 1998. A nonparametric method for automatic correction of intensity nonuniformity in MRI data. IEEE Trans. Med. Im. 17 (1), 87–97.

Szekeley, G., Gerig, G., 2000. Model-based segmentation of radiological images. KI Künstliche Intelligenz 3 (00), 18–23.

Vincent, L., Soille, P., Jun. 1991. Watersheds in digital spaces: An efficient algorithm based on immersion simulations. IEEE PAMI 13 (6), 583–598.

Wells, W. M., Grimson, W. E. L., Kikins, R., Jolesz, F. A., 1996. Adaptive segmentation of MRI data. IEEE Trans. Med. Im. 15 (4), 429–442.

Winkler, G., Aurich, V., Hahn, K., Martin, A., Rodenacker, K., 1999. Noise reduction in images: Some recent edge-preserving methods. Pattern Recognition and Image Analysis: Advances in Mathematical Theory and Applications 9 (4), 749–766.

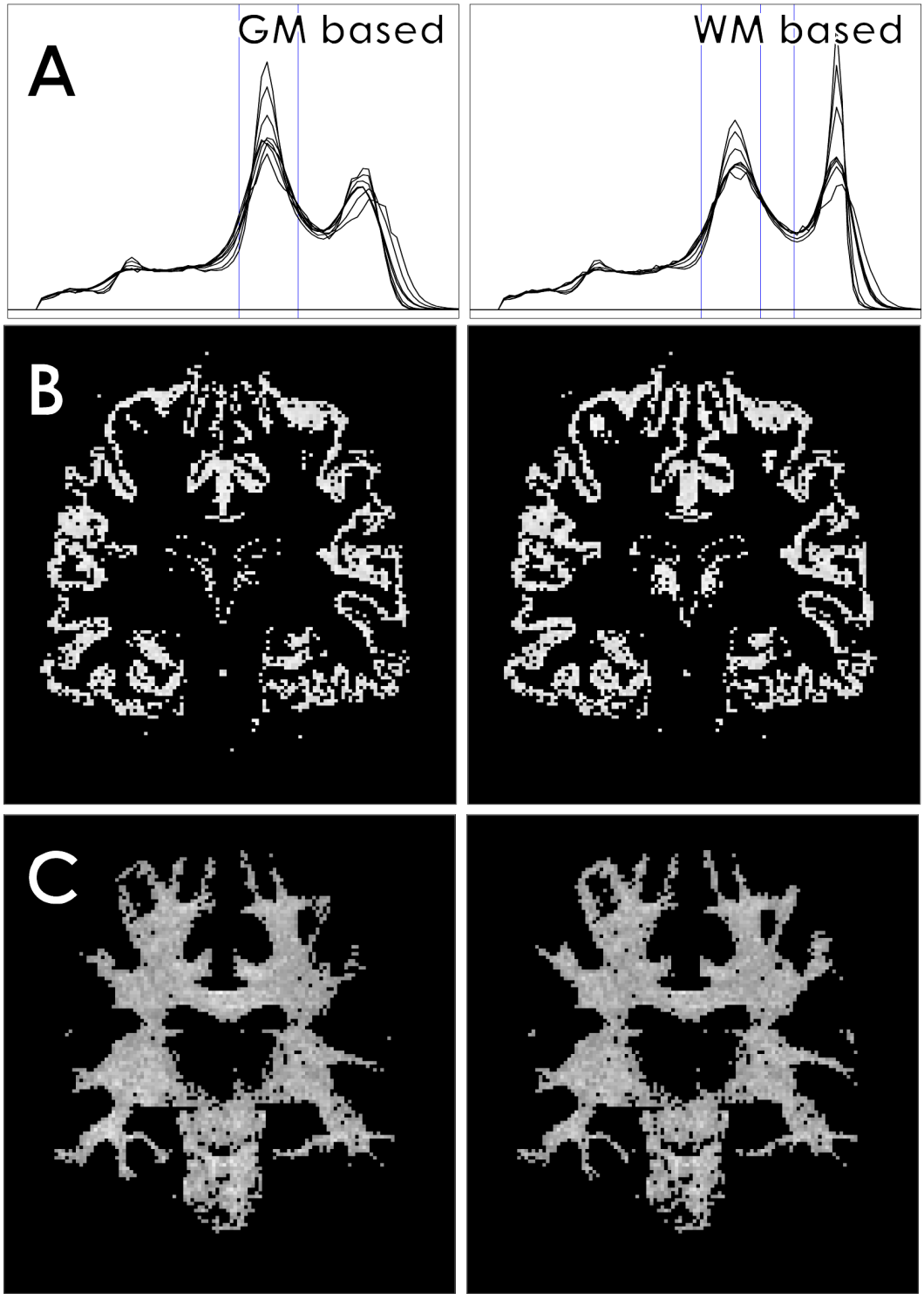

Fig. 11. Panel A: global intensity histograms of a representative brain for GM (left) and WM (right) based distortion corrections and smoothing, see text for details. B and C: GM and WM training sets in a coronal slice. Left panels for the 1^{st} irregular bias correction, right panels after the 4^{th} iteration. For horizontal panels the same thresholds are applied.

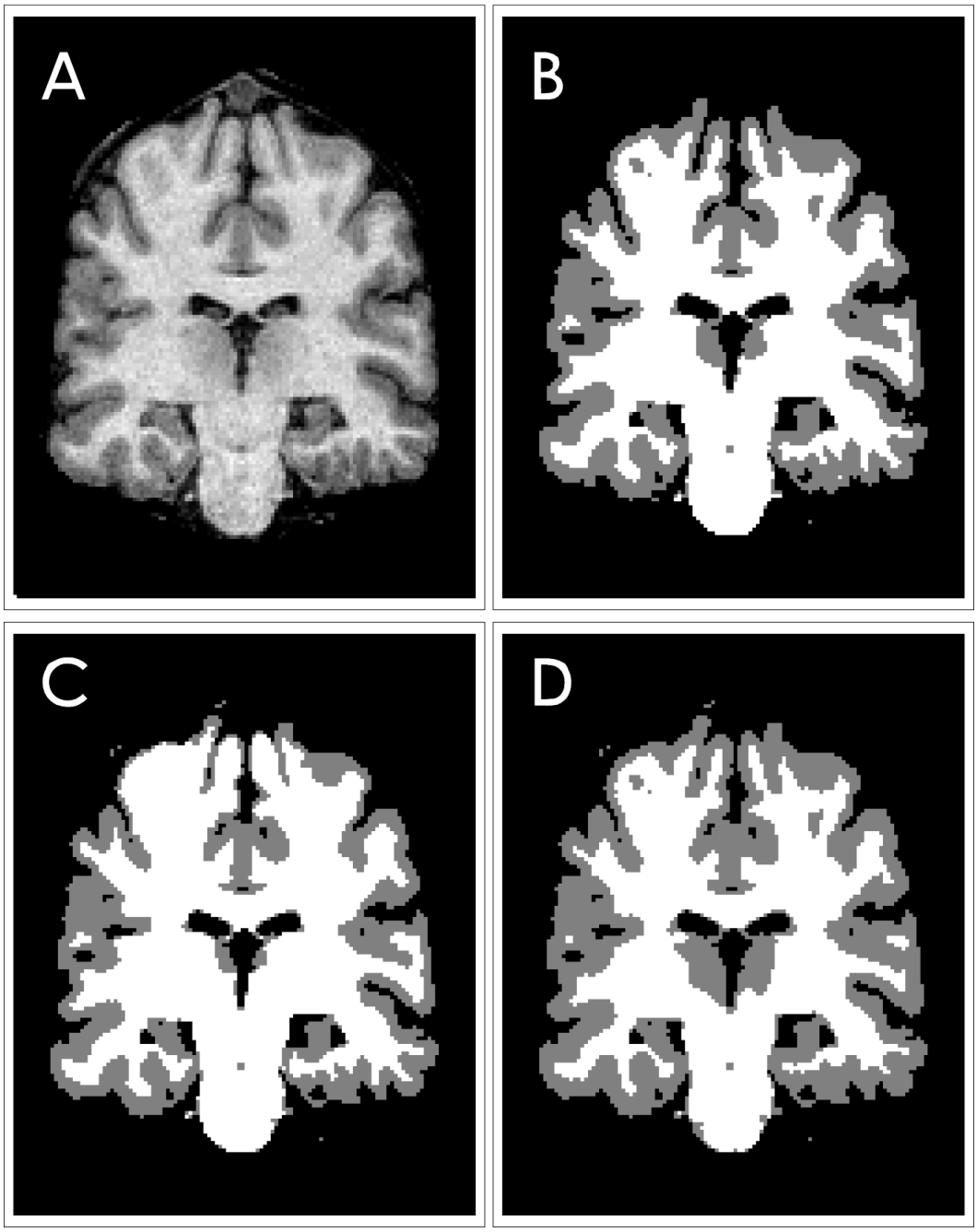

Fig. 12. Panel A: raw data from a representative brain; B: segmentation result based on GM; C: segmentation result based on WM, thresholds adjusted in such a way that the lower brain region is equivalent to the GM based segmentation; D: segmentation result based on WM, thresholds adjusted in such a way that the upper brain region is equivalent to the GM based segmentation (all segmentations without regridding)

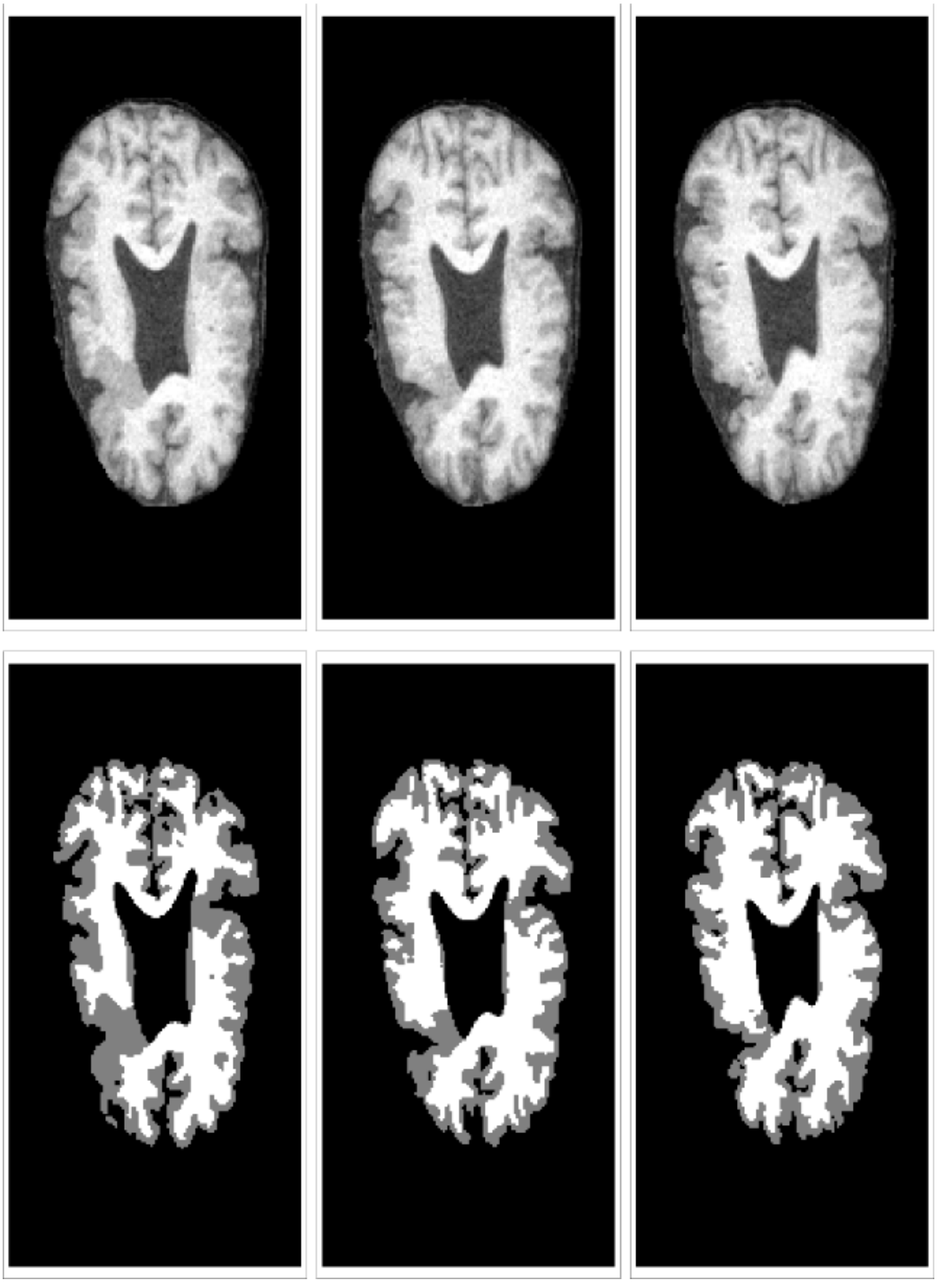

Fig. 13. Neighboring axial slices of a severely malformed brain, see text for details. Upper panels raw data, lower panels segmentation results